

Supplementary Information

**Mixing Oil and Water with Ionic Liquids: Bicontinuous Microemulsions
Under Confinement**

Hojun Kim^{a,b,§}, Mengwei Han^{c,§}, Sarith R. Bandara^a, Rosa M. Espinosa-Marzal^{c,*}, Cecilia Leal^{a,*}

^aDepartment of Materials Science and Engineering, University of Illinois at Urbana-Champaign, IL-61801
Urbana, USA

^bCenter for Biomaterials, Biomedical Research Institute, Korea Institute of Science and Technology
(KIST), Seoul, Republic of Korea

^cDepartment of Civil and Environmental Engineering, University of Illinois at Urbana-Champaign, IL-
61801 Urbana, USA

[§]Contributed equally

* Corresponding authors: cecilial@illinois.edu and rosae@illinois.edu

Materials and Methods

Decane, dodecane, and hexadecane, and trihexyl(tetradecyl)phosphonium chloride (>95 % purity determined by NMR) were purchased from Sigma Aldrich (MO, USA) and used without any further purification. Deionized water was obtained from Direct-Q Water Purification System (MilliporeSigma, MA, USA). Capillaries (1.5 mm O.D., wall thickness <0.1 mm) were purchased from Hilgenberg (Germany).

The microemulsion was prepared by mixi

ng water, oil, and ionic liquid (IL) in vials at the selected compositions (Figures 1 and S2). The volume of each component was added to a glass vial in the order of increasing density (oil -> IL -> water) (all chemicals were used without further purification). Afterwards, it was vortexed at high speed for 10 minutes and stored for a week at 45°C to achieve equilibrium. The middle phase of the Winsor type III (water/IL/oil = 75/5/20 mole ratio) was extracted and used for SWAXS and SFA measurements.

Microemulsion samples were transferred to quartz capillaries without centrifugation for SWAXS scans. Once the solution was transferred to the top of the capillary, it was gently shaken by hand until it reached the bottom of the capillary. The solutions were incubated for another week to achieve equilibrium before the measurement. SAXS scans were primarily performed with a home built (Forvis Technologies, CA, USA) SAXS instrument. The instrument is composed of a Xenocs Genix3D Cu-K α X-ray source (1.54 Å /8 keV), with low divergence of about 1.3 mrad. 2D diffraction data were radially averaged upon acquisition on a Pilatus 300 K 20 Hz hybrid pixel detector (Dectris, Switzerland) and integrated using FIT2D software (<http://www.esrf.eu/computing/scientific/FIT2D>) from the European synchrotron research facility. High resolution SWAXS data was collected from the beamline 12-ID-B, Advanced Photon Source at Argonne National Lab for detailed structural studies of the microemulsion. The synchrotron source has an average photon energy of 14 keV with full width of half maximum beam size of 300 μ m x 20 μ m (Horizontal x Vertical).

Force measurements were conducted with a Surface Forces Apparatus (SFA).¹ The mica surfaces used in the SFA experiments were prepared by manually cleaving ruby mica of optical quality grade # 1 (S&J Trading Inc, NY, USA). Freshly cleaved mica with a uniform thickness of 2-5 μm was cut into 8 mm by 8 mm pieces with surgical scissors. To avoid possible contamination, the preparation was done in a class-100 laminar-flow cabinet. The two mica surfaces were back-coated with a semitransparent layer of silver (40 nm) and glued onto two curved glass lenses (radius = 20 mm) with their optical axis oriented along the cylindrical axis of the lenses. Resin glue (EPON1004F) was melted at 140 °C on the glass lens, on which the back-silvered mica sheet was deposited with the silvered side facing the glue. Then, the lenses were immediately mounted in the eSFA cell with their cylindrical axes perpendicular to each other. Prior to each experiment, the thickness of the mica sheets was determined by making direct mica-mica contact in a dry N_2 atmosphere.

The absolute separation between the two mica surfaces (D) is measured in an SFA by multiple beam interferometry.¹⁻² In our extended version of the SFA, the transmitted spectrum of a beam of white light is analyzed by a numerical, fast-spectral correlation algorithm, which simultaneously determines both the surface separation with subnanometer precision and the refractive index of the sandwiched medium between the mica surfaces at the point of closest approach (PCA) in real-time.² Further, one of the lenses is connected to a spring, whose spring constant was selected to be 2364 ± 60 N/m in this study, and its deflection (ΔD) is used to calculate the surface force (F) across the confined medium between the two mica surfaces. Modifications have been made to improve the precision, resolution, and mechanical and thermal stability of the SFA,²⁻³ which lead to a measuring precision of D of ~ 30 pm, whereas the mechanical drift is reduced to less than 10^{-3} micron per minute. A resistive heater, coupled with a circulating cooling bath, effectively reduces the temperature variation to ± 0.05 °C around the selected value. Quasi-equilibrium force-separation curves are measured by approaching and separating one of the surfaces at a constant speed of 0.5 nm/s by means of a piezoelectric actuator (Physik Instrumenten, Germany).

The prepared water-IL-hexadecane mixtures were equilibrated at room temperature for one week before the middle phase of the stratified mixture was extracted and transferred to a sealed vial. Another week was given for the middle phase to fully stabilize before SFA measurements were conducted. Then, 100 μL of the microemulsion were transferred to the gap between the mica surfaces in the SFA cell using a syringe. The fact that the microemulsion is thermodynamically stable and has a calculated bending modulus of $\sim 0.2k\text{BT}$, makes us confident that the microemulsion recovers from any possible deformation by shear forces at the syringe. Throughout the experiments, the system was in equilibrium with ambient air, with a humidity of $\sim 32\pm 3\%$. Purging of the SFA cell with N_2 was avoided during the measurement, since preliminary tests showed a volume reduction of the microemulsion likely as a result of the loss of water. The surface-force measurements were conducted at three different temperatures, 17, 25, and 40 $^\circ\text{C}$. After a change of temperature, at least 8 hours were given for re-equilibration. Reference measurements were conducted on the oil phase (hexadecane with dissolved $\text{P}_{66614}\text{Cl}$) at 25 $^\circ\text{C}$. Force measurements in neat $\text{P}_{66614}\text{Cl}$ were not successful due to the high viscosity of the IL, which led to a large hydrodynamic force even at the slowest piezo velocities that prevented the measurement of equilibrium surface forces; squeeze-out of layers was not observed. The molecular structures of $\text{P}_{66614}\text{Cl}$ and of hexadecane are shown in Figure S1. To determine the dimensions of the molecules, a molecular-mechanics calculation of the optimized geometry was carried out with Avogadro (software version 1.2.0) using a MMFF94 force-field model.

In separate measurements, the microemulsion was deposited onto a freshly cleaved mica surface for imaging with an atomic force microscope (JPK, Germany). The system was equilibrated for 30 minutes to minimize thermal and mechanical drifts. The microemulsion-mica interface was imaged with a sharp silicon tip (spring constant=0.60 N/m) at room temperature (25 $^\circ\text{C}$) and ambient humidity ($\sim 32\%$ RH) using the Quantitative Imaging (QI) mode. In the QI mode, a force-separation curve is measured on each pixel on a 100 nm by 100 nm area. One single image was taken in ~ 2 hrs. The force-separation curves were then analyzed and convoluted into topography (determined by the end point of each approach) and stiffness (slope) images, and the individual force-separation curves were extracted and evaluated separately.

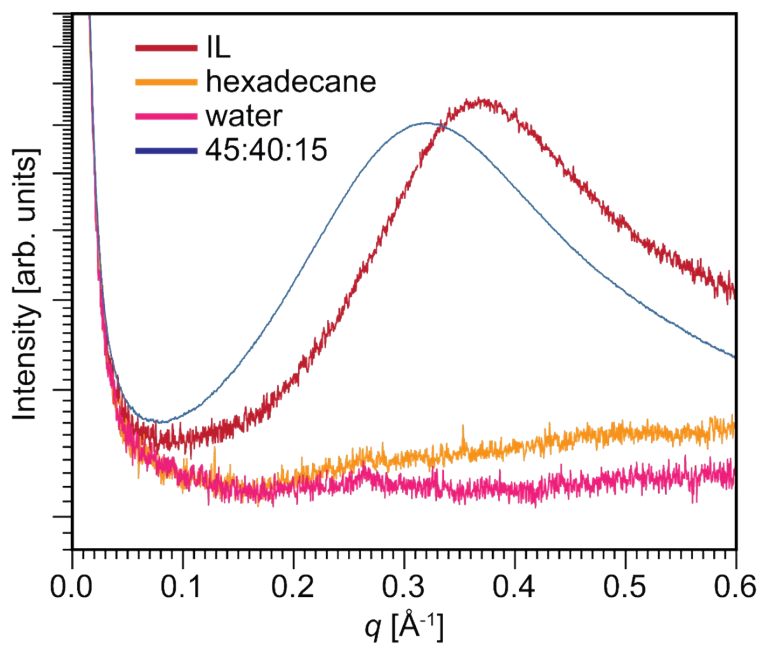
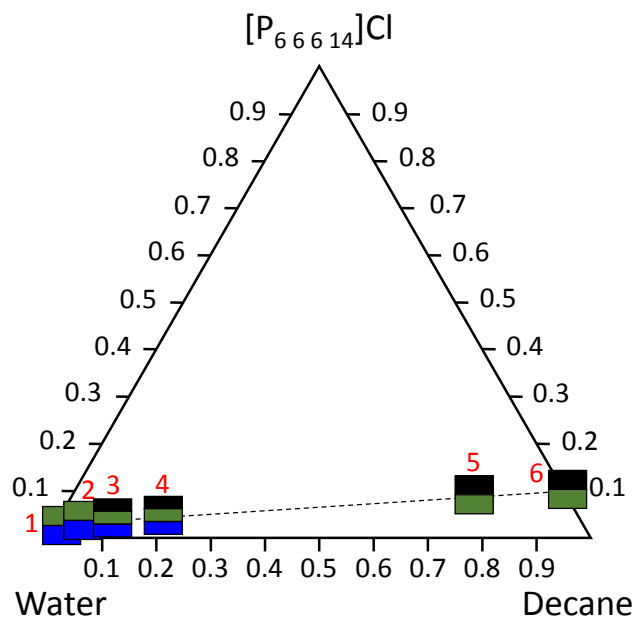
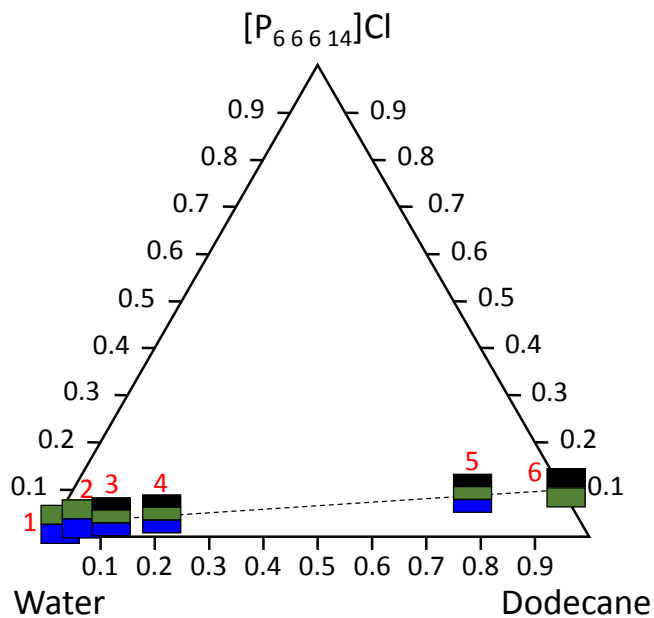


Figure S1. SAXS scans of pure IL, hexadecane, water and a single phase ($[\text{P}_{66614}]\text{Cl}$ / water / hexadecane = 0.40 / 0.45 / 0.15, mole ratio) showing no liquid crystalline order. Right image is the single solution.



| Sample Number | Global Composition (Water/IL/Oil) | Number of Phases |
|---------------|-----------------------------------|------------------|
| 1 | 97/0/3 | 2 |
| 2 | 95/2.5/2.5 | 2 |
| 3 | 87.5/2.5/10 | 3 |
| 4 | 75/5/20 | 3 |
| 5 | 14.2/8.8/77 | 2 |
| 6 | 0/10/90 | 2 |



| Sample Number | Global Composition (Water/IL/Oil) | Number of Phases |
|---------------|-----------------------------------|------------------|
| 1 | 97/0/3 | 2 |
| 2 | 95/2.5/2.5 | 2 |
| 3 | 87.5/2.5/10 | 3 |
| 4 | 75/5/20 | 3 |
| 5 | 14.2/8.8/77 | 3 |
| 6 | 0/10/90 | 2 |

Figure S2. Ternary phase diagram and global compositions of decane (top) and dodecane (bottom) based water/IL/oil mixtures. A longer alkyl tail of the oil molecules leads to the expansion of the microemulsion phase space in Winsor type III system.

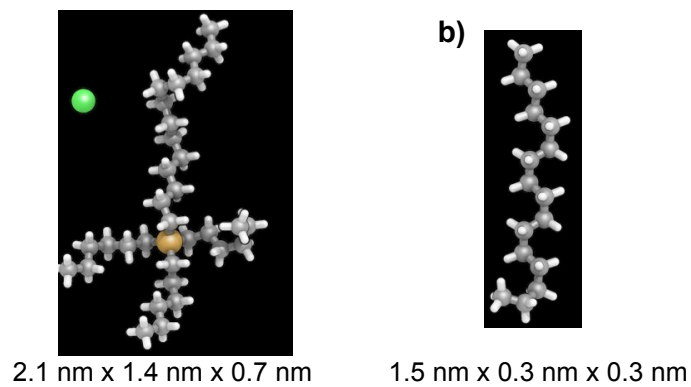


Figure S3. Molecular dimensions of a) $P_{66614}Cl$ and b) hexadecane. The geometry is optimized by Avogadro, with the MMFF94s force field.

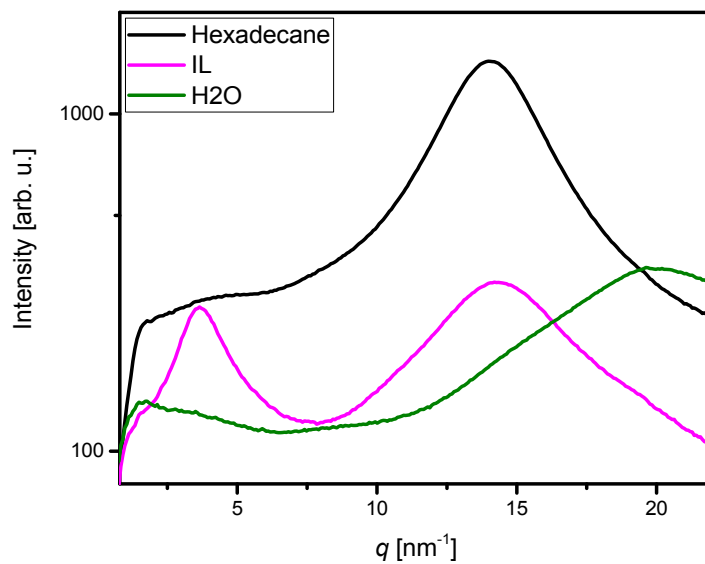


Figure S4. WAXS scans of pure hexadecane, $P_{66614}Cl$ and water.

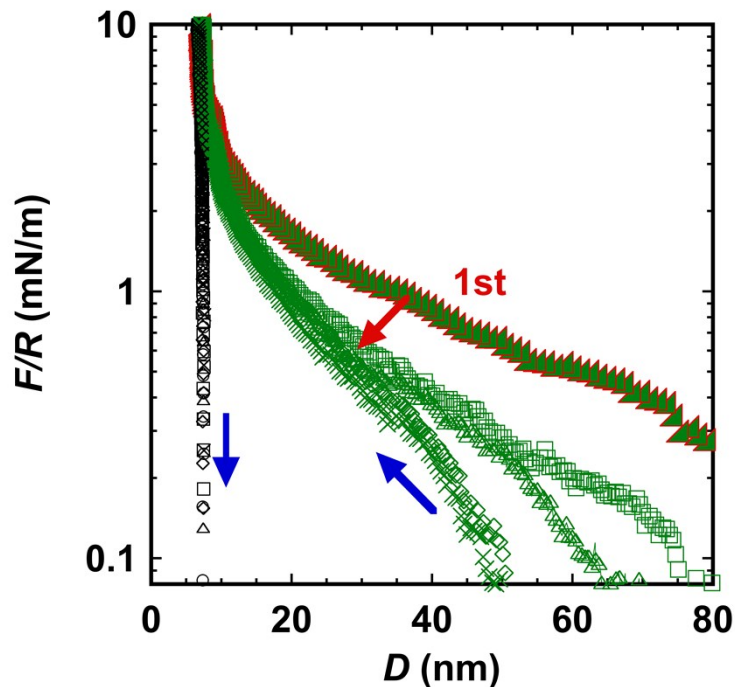


Figure S5. Force-distance curves in the microemulsion at 25°C measured during approach and separation of the mica surfaces at 0.5 nm/s with the SFA. The force-distance curve measured during the first approach of the surfaces is represented with filled green triangles, whereas the subsequent force-distance curves are represented with empty green symbols; the red arrow highlights the change of the force from the first to the subsequent approaches. The force-distance curves measured upon separation of the surfaces are shown with black symbols; there is no difference between first and subsequent force-distance curves upon separation. The hysteresis between approach and separation originates from the significant adhesion.

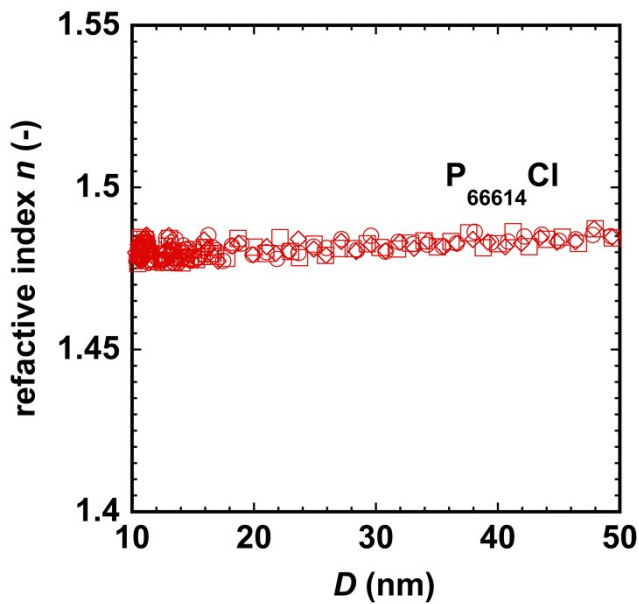


Figure S6. Refractive index (n) of $P_{66614}Cl$ as a function of the separation between the mica surfaces measured with the SFA. An average value of 1.485 is assumed for the following calculation.

Composition of the microemulsion based on the refractive index

The refractive index n_m of the microemulsion can be determined through its composition (obtained by SWAXS). The microemulsion consist of microdomains of IL-water (refractive index n_{ILW}) with a volume fraction $(1 - t)$ and oil microdomains (refractive index n_o) with a volume fraction t . Hence, the refractive index of the microemulsion is given by:⁴

$$n_m^2 = \frac{n_o^2 n_{ILW}^2}{t n_o^2 + (1 - t) n_{ILW}^2}$$

The measured refractive index of the microemulsion is $n_m \sim 1.46$ (Figure 3b). Assuming that the refractive index of the IL-water microdomains is mainly that measured for the pure IL ($n \sim 1.485$, Figure S4), a volume fraction of $t \sim 0.51$ is obtained for the oil phase.

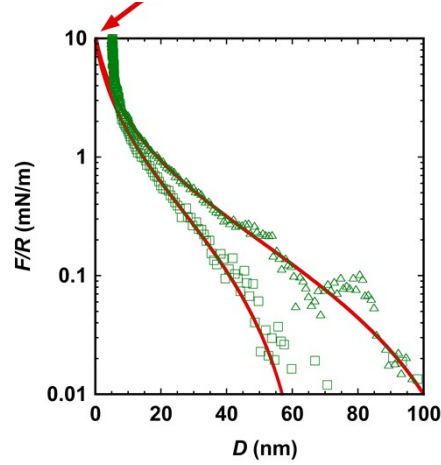


Figure S7. Force-distance curves in the microemulsion measured at 25°C. The repulsive force between surfaces in the microemulsion is thus compared to the theoretical force between two polymer layers using the scaling formalism developed by Alexander and de Gennes:⁷

$$\frac{F}{R} = \frac{8\pi}{35} k_B T \frac{2H}{d_m^3} \left[7 \left(\frac{D - 2D_0}{2H} \right)^{-\frac{5}{4}} + 5 \left(\frac{D - 2D_0}{2H} \right)^{\frac{7}{4}} - 12 \right]$$

Eq. (S1)

where d_m is the characteristic length representing the distance between the protruding microdomains, $2H$ the onset of the repulsion and $2D_0$ the position of the hard wall. Although developed specifically to model terminally grafted polymer brushes and even though the thermodynamics are not correctly captured using such a model for our system, the form of the resulting steric force upon compression is similar for end-grafted or adsorbed polymer layers at low grafting densities.⁸ To achieve a good fit to the experimental data at large separations, however, it is necessary to assume an unrealistic hard wall at $2D_0 \sim 0$ nm, instead of the hard wall observed in experiments (see arrow). This suggests that the model is not appropriate, and therefore, the protrusion model is preferred. Nevertheless, the lines show the fit of Eq. (S1) to the experimental results. The estimated spacing between the microdomains protruding from the surface d_m is 19.3(4.6), 18.1(5.2) and 17.4(4.9) nm at 17, 25 and 40 °C, respectively. Importantly, d_m is much larger than obtained with the protrusion model, which is reasonable, since the osmotic limit in the protrusion model assumes the lack of interactions between the protrusions, whereas in the Alexander and de Gennes, the protrusions need to be further away for these interactions to become negligible. Other models for surface

forces characteristic of amphiphilic systems, such as the undulation force ($F/R \sim D^{-2}$), do not describe well our data.

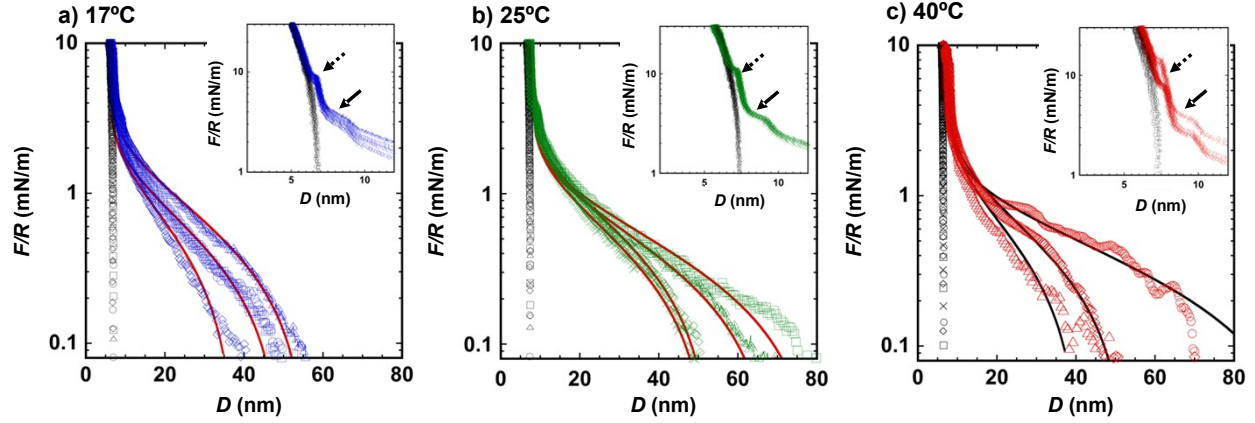


Figure S8. Force-distance curves measured in the microemulsion at three different temperatures (17, 25 and 40 °C). The lines show the fit of Eq. (1) -the protrusion model- to the experimental results. The estimated spacing d_m between the microdomains protruding from the surface is 8.1(2.5), 9.0(1.2) and 8.6(1.1) nm at 17, 25 and 40 °C, respectively. The insets show the steps superposed to the short-range force. The corresponding average thickness of the resolved steps at the selected temperatures 17, 25 and 40 °C was determined across different experiments with different pairs of mica surfaces; Δ_1 is 4.2(0.4), 4.0(0.2) and 4.9(0.6) Å (dashed arrow) and Δ_2 is 2.3(0.1), 2.4(0.2) and 2.5(0.1) nm (full arrow) at 17, 25 and 40 °C, respectively. The compressibility modulus of the larger layer is 1.2(0.2), 1.4 (0.2) and 1.9 (0.2) MPa. at 17, 25 and 40 °C, respectively.

It appears that the decrease in temperature reduces the variability of the long-range repulsive force, while the onset remains always larger than ~ 30 nm. The increasing spread at 40 °C is consistent with the greater thermal fluctuations expected in the microemulsion at higher temperatures. In contrast, the short-range surface forces (inset) are in quantitative agreement at the three temperatures, as reported for other short-range structural forces (e.g. for molecular liquids).³⁶ Only small changes of the structural parameters with temperature are observed.

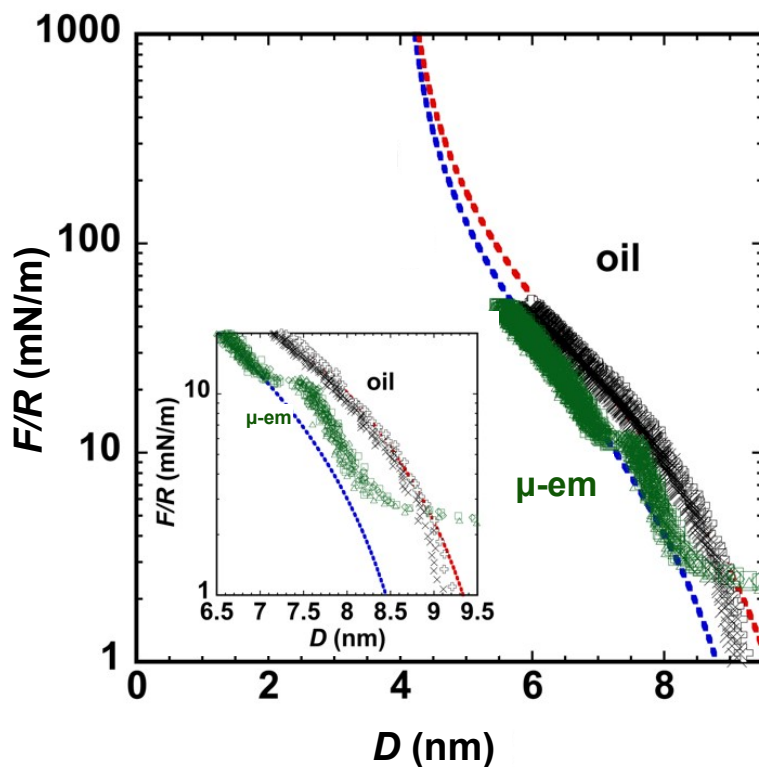


Figure S9. Short range force-distance curves in the microemulsion and in the oil phase at 25°C. The short-range repulsive force between surfaces in the microemulsion (μ -em) can be described as the steric interaction between the flexible head groups of the cations on opposite surfaces. The repulsion results from the restriction of the configurational entropy of the head groups, that is, as an entropic loss. Such an interaction can be approximately described as a brush-like repulsive force, according to Eq. (S1),⁹ and hence, it can be compared to the theoretical force between two polymer layers using the scaling formalism developed by Alexander and de Gennes.⁷ The fitting parameters are $D_0 \sim 4$ -5 nm as the incompressible film thickness (hard wall), and a spacing between the headgroups of $d_m \sim 1.7$ nm in the oil phase and 1.4 (0.2) nm in the microemulsion, which agrees well with the dimension of the head of the phosphonium cation.

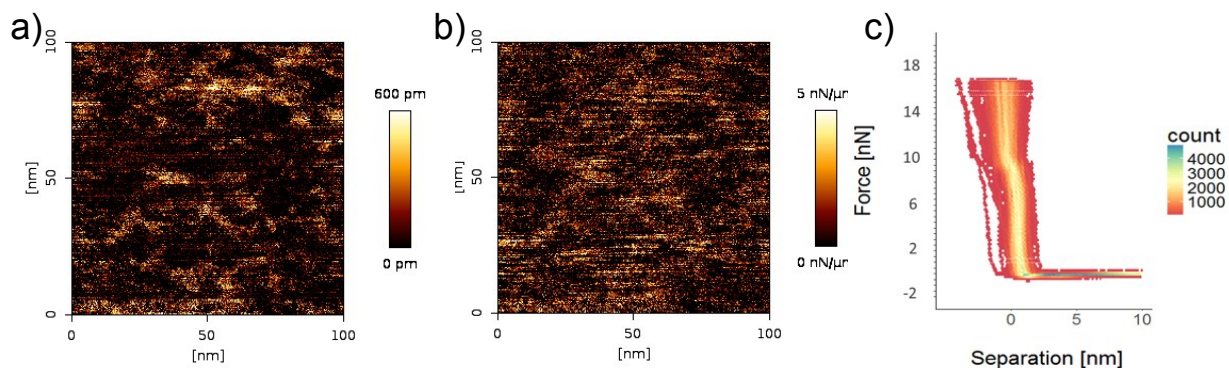


Figure S10. AFM images of a freshly cleaved mica surface immersed in the microemulsion. (a) Interfacial topography measured in QI mode. (b) Interfacial stiffness. (c) Bivariate histogram representing 64 superposed force-distance curves corresponding to the image shown in (a). A step with a thickness $\Delta \sim 8.7(1)$ Å is reproducibly resolved at a load of $9(0.2)$ nN.

The topography (a) and stiffness (b) images do not show the mesostructure of the microemulsion likely because the AFM tip displaces it when approaching to the surface. Based on our previous work with imidazolium ILs⁵, the step in the force-separation curves occurs when the tip pushes through an interfacial monolayer of ions. Here, it is likely that the tip strongly compresses the surface-adsorbed IL film and it pushes away one of the cation monolayers (with neutralizing anions), while the second cation monolayer may still remain between the tip and the surface⁵. The thickness of the layer is smaller than the length of the cation (~ 2.1 nm) shown in Figure S1. This can originate from the compression applied with the tip. It is also possible that the cation adopts a tilted orientation at the solid-liquid interface or a different molecular configuration (e.g. more flattened hexyl chains). Higher forces could resolve more strongly adsorbed ion layers, but they were not applied here to avoid the damage of the tip. Nevertheless, the push-through force is significantly higher than reported for other ILs adsorbed on mica,⁶ which reflects either the strong adsorption of $P_{66614}Cl$ to mica, the densely packed structure due to the strong association between the long alkyl chains, or a combination of both. In the SFA experiments, much smaller pressures are applied (6 MPa in SFA vs. ~ 2 GPa in AFM experiments), and therefore, it is reasonable to assume that the fluid film that remains confined between the mica surfaces at the maximum load is mainly composed of the IL constituent.

References

1. Israelachvili, J. N., Thin film studies using multiple-beam interferometry. *Journal of Colloid and Interface Science* **1973**, *44* (2), 259-272.
2. Heuberger, M., The extended surface forces apparatus. Part I. Fast spectral correlation interferometry. *Review of Scientific Instruments* **2001**, *72* (3), 1700-1707.
3. Heuberger, M.; Vanicek, J.; Zäch, M., The extended surface forces apparatus. II. Precision temperature control. *Review of Scientific Instruments* **2001**, *72* (9), 3556-3560.
4. Kekicheff, P.; Richetti, P.; Christenson, H. K., Structure and elastic properties of lamellar mesophases from direct force measurements. *Langmuir* **1991**, *7* (9), 1874-1879.
5. Sheehan, A.; Jurado, L. A.; Ramakrishna, S. N.; Arcifa, A.; Rossi, A.; Spencer, N. D.; Espinosa-Marzal, R. M., Layering of ionic liquids on rough surfaces. *Nanoscale* **2016**, *8* (7), 4094-106.
6. Atkin, R.; Warr, G. G., Structure in Confined Room-Temperature Ionic Liquids. *The Journal of Physical Chemistry C* **2007**, *111* (13), 5162-5168.
7. de Gennes, P. G., Polymers at an interface; a simplified view. *Advances in Colloid and Interface Science* **1987**, *27* (3), 189-209.
8. Israelachvili, J. N., *Intermolecular and Surface Forces: Revised Third Edition*. Elsevier Science: 2011.
9. Israelachvili, J. N.; Wennerstroem, H., Entropic forces between amphiphilic surfaces in liquids. *The Journal of Physical Chemistry* **1992**, *96* (2), 520-531.